Confinement Induced Splay-to-Bend Transition of Colloidal Rods

Oliver J. Dammone,[1] Ioannis Zacharoudiou,[2] Roel P. A. Dullens,[1] Julia M. Yeomans,[2]
M. P. Lettinga,[3] and Dirk G. A. L. Aarts[1]

[1]*Department of Chemistry, Physical and Theoretical Chemistry Laboratory, University of Oxford, South Parks Road, Oxford OX1 3QZ, United Kingdom*

[2]*Rudolf Peierls Centre for Theoretical Physics, University of Oxford, 1 Keble Road, OX1 3NP, United Kingdom*

[3]*Institut für Festkörperforschung, Forschungszentrum Jülich, 52425 Jülich, Germany*

(Received 12 March 2012; published 5 September 2012)

We study the nematic phase of rodlike fd-virus particles confined to channels with wedge-structured walls. Using laser scanning confocal microscopy we observe a splay-to-bend transition at the single particle level as a function of the wedge opening angle. Lattice Boltzmann simulations reveal the underlying origin of the transition and its dependence on nematic elasticity and wedge geometry. Our combined work provides a simple method to estimate the splay-to-bend elasticity ratios of the virus and offers a way to control the position of defects through the confining boundary conditions.

DOI: 10.1103/PhysRevLett.109.108303 PACS numbers: 82.70.Dd, 02.70.−c, 61.30.−v

Packing and confinement problems emerge in fields ranging from biology to engineering. In biological systems the organization of the cell is determined, among other things, by the packing of fibril-like particles (actin filaments, DNA) [1,2]. An example of the subtlety of packing phenomena is the plethora of liquid crystalline phases that can be found in arrangements of anisotropic particles by increasing concentration [3,4]. Confinement of liquid crystals adds to the complexity, since the interactions of the particles with the walls may lead to structures that compete with those formed in the bulk [5,6]. Many of the next generation liquid crystal display devices exploit this interplay by using structured or patterned surfaces as an essential element of their design [7,8]. Very recently, the ordering at sawtooth structures has been studied theoretically within a Landau–de Gennes framework [9,10], with a focus on the wetting behavior. In this Letter, in a combined experimental and theoretical effort, we show the rich phenomenology that emerges when confining a nematic liquid crystal to a microfluidic channel with a wedge structured wall. We seek to disentangle how the wedge geometry and elasticity of the fd-virus' nematic phase determine the adopted deformation in the wedge. We introduce a new method for estimating elastic constants suitable to colloidal and biological systems, as an alternative to previous methods using magnetic fields [11] or light scattering [12]. Specifically, we determine the transition from a splay to a bend director field, with increasing wedge angle.

We use the fd-virus, which is an excellent model liquid crystal system for both static and dynamic behavior [13–16]. The virus' contour length and diameter are 0.88 μm and 6.6 nm, respectively. These dimensions allow for the 3D determination of the position and orientation of individual particles by means of laser scanning confocal microscopy (LSCM). Thus we obtain detailed mechanistic insights on a single particle level of the director field. Moreover, due to the relatively large size of the particles, we can study effects of wall structures that are, when translated to the scale of thermotropic liquid crystals, very small and inaccessible.

The particles were grown following standard protocols [17] and dispersed in 20 mM tris buffer at pH 8.15 with 100 mM NaCl and 15% EtOH. The ethanol was added to prevent the growth of bacteria. The virus concentration was 24 mg/ml, which is in the nematic phase. Of the particles 1% was fluorescently labeled with Alexa-488 NHS ester. The labeled particles were imaged by means of confocal microscopy using a Zeiss LSM 5 Exciter, 63x 1.4 NA oil-immersion objective. Microfluidic channels were constructed from UV glue (NOA 81) and bound to glass coverslips as described in the soft lithography protocols [18], which guaranteed sealing over the course of the experiment. One of the walls was structured with wedges with a range of opening angles, see Fig. 1(a). The radius of curvature of the tip of the wedge is smaller than 2.5 μm and the walls are smooth on the colloidal length scale (~ 1 μm). The measurement range was 40°–100° in steps of 10°. The height of the channels was 10 μm, which is smaller than the cholesteric pitch [19], giving 'pseudo 2D' confinement. This was confirmed by three dimensional LSCM scans. Due to the thin samples polarization microscopy was not possible. The width of the channels is characterized by h_c and h_w [Fig. 1(a)]. We used $h_c = 500$ μm and $h_w = 75$, 750 and 1125 μm.

The structured microfluidic channels were filled by capillary action. Directly before filling, the channels were plasma cleaned, which changes the hydrophilicity of the channels and offers a way to control the speed of filling. This enabled us to set the initial conditions of the experiment due to the coupling between the nematic director and flow: low filling speeds created an initial disordered configuration, while high filling speeds resulted in the rods

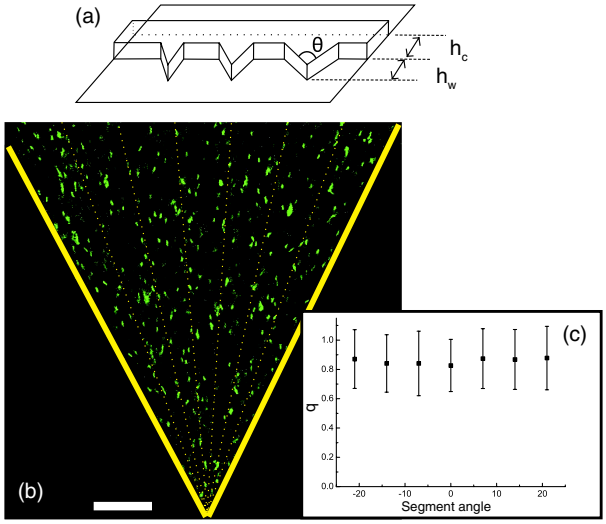

FIG. 1 (color online). (a) Geometry of the microfluidic channel. (b) Microscopy picture of the nematic phase in the splay deformation, obtained by overlaying 7 LSCM images. Only the fluorescent fd-virus particles are visible. Scale bar is 10 μm. See Supplemental Material for movie [21]. (c) Plot of order parameter versus segment angle for the movie corresponding to the image in (b). The segments are indicated in (b) by the overlaid dashed lines.

immediately adopting metastable aligned deformations, which only slowly found equilibrium [20]. We filled the channels slowly and from a disordered configuration, the equilibrium was reached within a couple of hours.

Figure 1(b) displays a LSCM image of the fluorescently labeled rods in a splay deformation. The nematic deformations are clearly seen from movies in which the rods move along the director lines, see Supplemental Material [21]. Tracking the particles close to the walls, we verified no rods were sticking to the walls. To quantify the LSCM images, we first use image analysis software to identify each rod's position and orientation [22]. Figure 2(a) shows the experimental director fields, obtained by dividing a series of ten 202×202 μm LSCM images into squares of area 13.5×13.5 μm and then averaging the orientation of the rods in each square. The average number of rods per square is 50 rods, and the standard deviation in the orientation is 10%. The lapse time between images was 30 seconds which is longer than the typical self-diffusion time, ensuring the images are statistically independent. In addition, for splay deformations we calculated the order parameter q [3] in piecewise segments across the wedge. We find that the order parameter is constant across the wedge, which indicates strong planar anchoring; see Fig. 1(c).

We observe splay deformations, accompanied by a defect in the bulk of the wedge, below 70° and bend deformations above 80°. Clearly, the location of the splay-to-bend transition will depend on the ratios of the splay (K_1) to bend (K_3) elasticity. Starting from a simplified picture we may assume the following: In going from an opening angle of 180°, i.e., a flat wall, to an opening angle of 0° we go from a bend to a splay deformation. For the semi-flexible fd-virus we expect $K_3/K_1 \approx 1$, from reported values of semiflexible liquid crystals [3,12,23]. Due to the underlying symmetry of the problem we would then expect the splay-to-bend transition to occur at 90°. Mottram also found the transition to occur at 90° by using a conformal mapping technique within the one constant approximation [24].

To elucidate our observations we performed numerical simulations taking the actual channel geometry into account. The simulations are based on the Beris-Edwards [25] model for liquid crystal hydrodynamics where the continuum equations of motion are written in terms of a tensor order parameter $Q_{\alpha\beta} = q(3n_\alpha n_\beta - \delta_{\alpha\beta})/2$. Its largest eigenvalue gives the nematic degree of order q and the corresponding eigenvector the director field $\hat{\mathbf{n}}$. The equilibrium properties of the liquid crystal are described by the Landau–de Gennes free energy [3,26]. This comprises a bulk term f_b and an elastic term f_{el}:

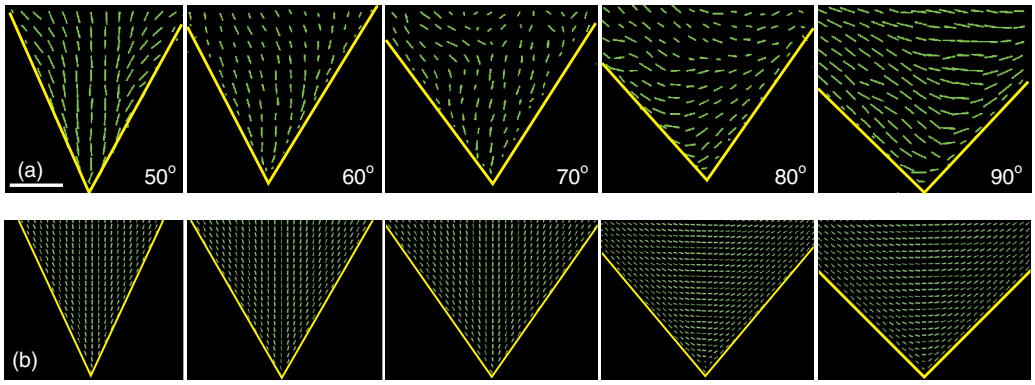

FIG. 2 (color online). Director field in the wedge for varying wedge angle $\theta = 50°$–$90°$: (a) Director fields from experiments, calculated by averaging over 10 images. Scale bar is 50 μm. (b) Director field from lattice Boltzmann simulations. In both cases the transition from a splay to a bend configuration occurs between 70°–80°.

$$f_b = A_0\left[\frac{1}{2}\left(1-\frac{\gamma}{3}\right)Q_{\alpha\beta}^2 - \frac{\gamma}{3}Q_{\alpha\beta}Q_{\beta\gamma}Q_{\gamma\alpha} + \frac{\gamma}{4}(Q_{\alpha\beta}^2)^2\right], \quad (1)$$

$$f_{\mathrm{el}} = \frac{L_1}{2}(\partial_\alpha Q_{\beta\gamma})^2 + \frac{L_2}{2}(\partial_\alpha Q_{\alpha\gamma})(\partial_\beta Q_{\beta\gamma}) + \frac{L_3}{2}Q_{\alpha\beta}(\partial_\alpha Q_{\gamma\epsilon})(\partial_\beta Q_{\gamma\epsilon}). \quad (2)$$

In Eq. (1), γ is a measure of the rod concentration, which sets the location of the first order isotropic-nematic transition to $\gamma = 2.7$ and the nematic degree of order, and A_0 is a constant. In Eq. (2), the prefactors L_n with $n = 1$, 2, or 3 are linear combinations of the Frank elastic constants, K_n [27]:

$$K_1 = \frac{9q^2}{4}(2L_1 + L_2 - qL_3), \qquad K_2 = \frac{9q^2}{4}(2L_1 - qL_3),$$
$$K_3 = \frac{9q^2}{4}(2L_1 + L_2 + 2qL_3). \quad (3)$$

The anchoring of the director on the walls is modeled by using a Rapini-Papoular-like surface free energy density, $f_s = W^{\mathrm{uni}}(Q_{\alpha\beta} - Q^0_{\alpha\beta})^2$, where W^{uni} denotes the uniform anchoring strength and $Q^0_{\alpha\beta} = q(3n^0_\alpha n^0_\beta - \delta_{\alpha\beta})/2$ corresponds to the preferred director orientation $\hat{\mathbf{n}}^{\mathbf{0}}$ imposed by the walls. The equations of motion are solved using a hybrid lattice Boltzmann scheme [28]. Although we report only results in equilibrium, solving the full hydrodynamic equations was found to be an efficient way of accessing the free energy minimum.

Apart from reproducing the geometry of the microchannel, there are several conditions that need to be fulfilled in order to match the experimental conditions. First, we keep the nematic degree of order q around 0.8 to match the ordering in the experiments. Second, the starting configuration is matched by choosing an isotropic configuration in the wedge ($q = 0$), and a nematic state with a horizontal director $\hat{\mathbf{n}}$ in the channel above the wedge. Third, we take $K_3/K_1 = 1$, as discussed earlier, and consider strong planar surface anchoring that leads to perfect alignment of the rods with the surfaces, as in the experiments. Finally, we approach the experimental situation by using $\xi_N/h_w \sim 1/100$. The nematic correlation length ξ_N sets the length scale for the variations in the nematic degree of order q. Experimentally, ξ_N is of order of the rod dimensions, i.e., $\sim\mu$m.

Figure 2 compares the director field obtained in experiment and simulation, showing very close agreement. In particular, both sets of data display a splay-to-bend transition at opening angles $\sim 70°$. This gives us the confidence to use the simulations to demonstrate the mechanism behind the transition, and its dependence on the details of the confinement geometry.

In the case of splay deformations, the inevitable frustration of the director field due to the horizontal configuration in the main channel leads to an $s = -1/2$ defect in the wedge. Figure 3(a) shows the numerical director profile at a wedge opening angle of 70°, close to the splay-to-bend transition. The rods adopt a splay deformation at the tip and a bend deformation at the top of the wedge resulting in an $s = -1/2$ defect. This is indeed observed in the experiments, see Fig. 3(b) and the accompanying movie [21] for images of the defect at the single particle level. The presence of this defect plays an important role in determining the stable director configuration. For a full understanding of the splay-to-bend transition, the complete geometry, including the top wall bounding the micro channel, needs to be considered, as is evident from Fig. 3.

Figure 4 shows experimental and simulation results for the relative position of the defect, defined as $\tilde{h} = z_d/h_w$ with z_d the height of the defect with respect to the tip, plotted as a function of the opening angle θ_w. Results are presented for different values of the ratio of channel height to wedge length $r_w = h_c/h_w$. For the largest wedge heights h_w multidomains (Schlieren-texture) may be present near the top of the wedge, which is suppressed for the small h_w. For small θ_w the defect lies close to the top of the wedge, marking the boundary between the splay ordering imposed

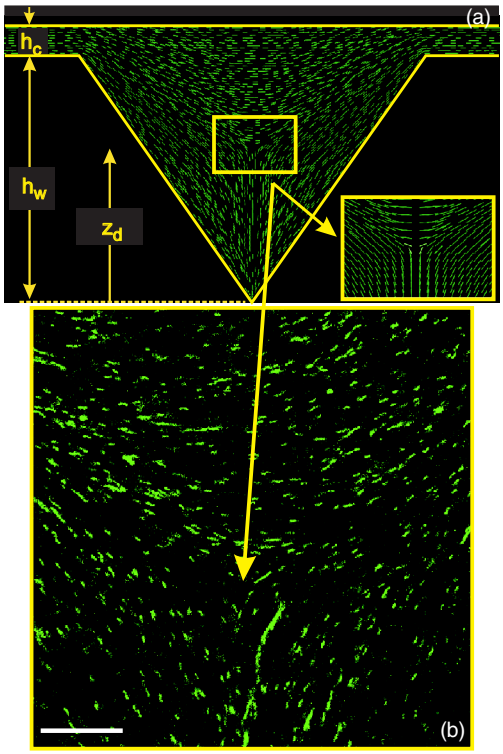

FIG. 3 (color online). (a) Director field from a simulation for a wedge angle of 70° showing a defect of strength $s = -1/2$, where the splay configuration meets the bend configuration. The inset shows a zoom of the defect. (b) Microscopy picture of the corresponding defect, obtained by overlaying 5 LSCM images. Only the fluorescent fd-virus particles are visible. Scale bar is 10 μm. See Supplemental Material for movie [21].

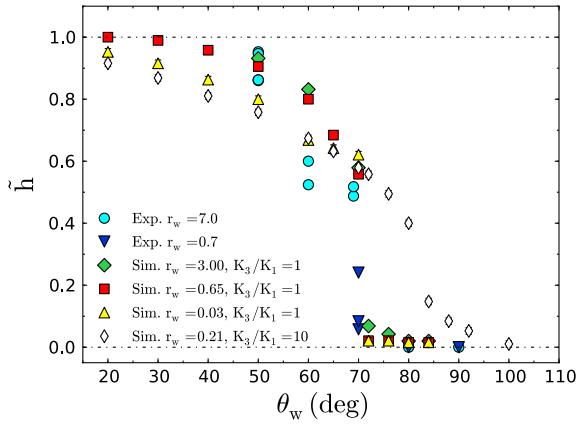

FIG. 4 (color online). The relative position of the defect within the wedge $\tilde{h} = z_d/h_w$ plotted as a function of the wedge angle θ_w, for varying channel geometries $r_w = h_c/h_w$. For an elasticity ratio $K_3/K_1 = 1$ ($L_1 = 0.139$; $L_2 = L_3 = 0$; $q = 0.8$) the splay-to-bend transition takes place at the same wedge opening angle, independent of the width of the microfluidic channel above the wedge. For $K_3/K_1 = 10$ ($L_1 = 0.423$; $L_2 = 0$; $L_3 = 0.791$; $q = 0.8$), however, the transition moves to a higher opening angle.

by the wedge and the horizontal nematic configuration imposed by the top channel boundary. With increasing wedge angle the splay deformation becomes less favorable, and the defect is pushed into the wedge by the dominance of the nematic order in the microchannel. This effect is more pronounced for the narrower channels for which the top wall has a stronger effect. This illustrates that the position of the defect can be controlled through the wedge and channel geometry. In Fig. 4, the curves converge as the wedge angle increases indicating that the defect has moved sufficiently far down into the wedge that it no longer feels the upper surface. An abrupt transition is observed just above 70° for all values of r_w. This corresponds to the splay-to-bend transition: for higher wedge angles the defect is no longer present and a bend deformation is adopted. The transition occurs when the energy of the splay configuration plus the energy of the defect becomes equal to the energy of the bend configuration. Here the transition occurs at an angle smaller than the predicted $\theta_w \sim 90°$ for an infinitely large wedge.

Fig. 4 shows that the transition is sharp and does not depend on r_w. As we encounter the splay-to-bend transition the main channel maintains its horizontal director field and, therefore, the location of the transition is determined mainly by the wedge. It is at first sight surprising that the transition occurs at an opening angle that is independent of h_w, the height of the wedge. However, this can be motivated by noting that the energy of the defect (per unit length and using the one elastic constant approximation) is given by $E_d = K\{\epsilon_d + \frac{\pi}{4}\ln(\frac{R}{r_c})\}$ [3], where the first term is the contribution from the core of the defect and R is the distance to the walls of the wedge. A lower cut-off r_c is introduced, which is related to the size of the defect core and can be approximated by the nematic correlation length ξ_N. The second term in the defect energy is proportional to the elastic constant K and depends logarithmically on the system size. The same is true for the energies of the splay and bend configurations [24]. Hence, given that we may ignore the first term in the defect energy, the splay-bend transition will be independent of the size of the wedge. The energetic contribution of the defect core ϵ_d can be quantified by the ratio of the nematic correlation length to the height of the wedge ξ_N/h_w. We expect that experimentally ξ_N is of order of the dimensions of the rods. Hence, $\xi_N/h_w \ll 1$ and ϵ_d is indeed negligible. (We find numerically that the transition can be shifted to higher opening angles due to the effect of the defect core energy, but this effect only becomes non-negligible for $h_w \sim 10$ rod lengths.)

Experimentally we measure a splay-bend transition between 70°–80°. Simulations show that increasing K_3/K_1 gives an increase in the angle of the splay-bend transition: 72° for $K_3/K_1 = 1$ and 82° for $K_3/K_1 = 4$. Moreover, for a fixed channel geometry the defect lies at a lower position in the wedge for increasing K_3/K_1. For $K_3/K_1 = 2$ the transition shifts to 76° but the position of the defect is lower than in the experiment. Thus, from the splay-bend transition angle and the defect height we estimate $K_3/K_1 \approx 1$.

To conclude, we have used laser scanning confocal microscopy to image the director field of a colloidal liquid crystalline virus on a single particle level. Thus, it was possible to directly observe the nematic ordering in a microchannel patterned with wedges of varying opening angle. The complex interplay between confinement, elasticities and surface anchoring led to a splay-to-bend transition mediated by a defect in the center of the wedge. Numerical results, in quantitative agreement with the experiments, enabled us to predict the position of the defect as a function of opening angle, and elucidate its role in the change of director structure. Our experiments have relevance to novel energy saving, liquid crystal devices [29] which rely on defect motion, and pinning to create bistable director configurations.

We thank Paul van der Schoot and Ronald Otten for useful discussions. This project was supported by the Royal Society.

[1] O. Medalia, I. Weber, A. Frangakis, D. Nicastro, G. Gerisch, and W. Baumeister, Science **298**, 1209 (2002).
[2] M. Soares e Silva, J. Alvarado, J. Nguyen, N. Georgoulia, B. M. Mulder, and G. H. Koenderink, Soft Matter **7**, 10631 (2011).
[3] P. G. de Gennes and J. Prost, *The Physics of Liquid Crystals* (Oxford University Press, Oxford, 1993), 2nd ed.

[4] E. Grelet, Phys. Rev. Lett. **100**, 168301 (2008).
[5] W.-J. Chung, J.-W. Oh, K. Kwak, B. Y. Lee, J. Meyer, E. Wang, A. Hexemer, and S.-W. Lee, Nature (London) **478**, 364 (2011).
[6] T. Gibaud, E. Barry, M. Zakhary, M. Henglin, A. Ward, Y. Yang, C. Berciu, R. Oldenbourg, D. Nicastro, R. Meyer, and Z. Dogic, Nature (London) **481**, 348 (2012).
[7] A. Majumdar, C. J. P. Newton, J. M. Robbins, and M. Zyskin, Phys. Rev. E **75**, 051703 (2007).
[8] A. J. Davidson, C. V. Brown, N. J. Mottram, S. Ladak, and C. R. Evans, Phys. Rev. E **81**, 051712 (2010).
[9] J. Romero-Enrique, C.-T. Pham, and P. Patrício, Phys. Rev. E **82**, 011707 (2010).
[10] P. Patrício, J. Romero-Enrique, N. Silvestre, N. Bernardino, and M. Telo da Gama, Mol. Phys. **109**, 1067 (2011).
[11] A. Hurd, S. Fraden, F. Lonberg, and R. B. Meyer, J. Phys. (Les Ulis, Fr.) **46**, 905 (1985).
[12] R. B. Meyer and S.-D. Lee, Phys. Rev. Lett. **61**, 947 (1988).
[13] M. P. Lettinga and E. Grelet, Phys. Rev. Lett. **99**, 197802 (2007).
[14] Z. Dogic, K. Purdy, E. Grelet, M. Adams, and S. Fraden, Phys. Rev. E **69**, 051702 (2004).
[15] E. Pouget, E. Grelet, and M. P. Lettinga, Phys. Rev. E **84**, 041704 (2011).
[16] F. Tombolato, A. Ferrarini, and E. Grelet, Phys. Rev. Lett. **96**, 258302 (2006).
[17] Z. Dogic and S. Fraden, in *Soft Matter*, edited by G. Gompper and M. Schick (Wiley-VCH, Weinheim, 2006), Vol 2, 1st ed.
[18] D. Bartolo, G. Degré, P. Nghe, and V. Studer, Lab Chip **8**, 274 (2008).
[19] Z. Dogic and S. Fraden, Langmuir **16**, 7820 (2000).
[20] M. P. Lettinga, Z. Dogic, H. Wang, and J. Vermant, Langmuir **21**, 8048 (2005).
[21] See Supplemental Material at http://link.aps.org/supplemental/10.1103/PhysRevLett.109.108303 for movies corresponding to Figs. 1(b) and 3(b).
[22] J. C. Crocker and D. G. Grier, J. Colloid Interface Sci. **179**, 298 (1996).
[23] E. Barry, D. Beller, and Z. Dogic, Soft Matter **5**, 2563 (2009).
[24] A. J. Davidson and N. J. Mottram, Eur. J. Appl. Math. **23**, 99 (2011).
[25] A. N. Beris and B. J. Edwards, *Thermodynamics of Flowing Systems: with Internal Microstructure*, Engineering Science Series (Oxford University Press, Oxford, 1994).
[26] S. F. Doi and M. Edwards, *The Theory of Polymer Dynamics* (Oxford University Press, Oxford, 1986).
[27] K. Schiele and S. Trimper, Phys. Status Solidi B **118**, 267 (1983).
[28] C. Denniston, E. Orlandini, and J. M. Yeomans, Phys. Rev. E **63**, 056702 (2001).
[29] C. Uche, S. J. Elston, and L. A. Parry-Jones, J. Phys. D **38**, 2283 (2005).